

# On the boundary conditions in tracer transport models for fractured porous underground formations

M. Coronado, J. Ramírez-Sabag, and O. Valdiviezo-Mijangos  
*Instituto Mexicano del Petróleo,*  
*Eje Central Lázaro Cárdenas 152, 07730 México D.F., Mexico,*  
*e-mail: mcoronad@imp.mx, jrsabag@imp.mx, ovaldivi@imp.mx*

Recibido el 24 de octubre de 2006; aceptado el 7 de junio de 2007

A boundary condition traditionally used in analytical models for tracer or contaminant pulse transport in porous underground formations gives the tracer concentration at the injection border as a discontinuous function in time. It has recently been shown that this condition leads to a physically improper pulse behavior. Models using sounder boundary conditions are already available for non-fractured porous media, but not for fractured media, where the traditional condition is commonly employed which can potentially lead to errors. We develop two new formulations to describe tracer tests in fractured media. They set conditions (i) on the total amount of injected tracer and (ii) on the tracer flow. The new formulations are compared against the traditional debatable model by examining tracer breakthrough curve differences. It has been found that they are important at small Peclet numbers. Differences are analyzed in two ways, by (a) employing typical model parameter values, and (b) fitting the three models to the same field tracer data set, and comparing the resulting model parameter values. In the first case the breakthrough curve difference has been quantified at 25%, and in the field tests considered in the second case it was from 1% to 10%. In general these discrepancies are small, but could become significant in some cases.

**Keywords:** Boundary conditions; tracer transport; porous media; fractured reservoirs.

Una condición de frontera usada tradicionalmente en modelos analíticos de transporte de un pulso de trazador o de contaminante en formaciones porosas subterráneas, establece la concentración de trazador en la frontera de inyección como una función discontinua en el tiempo. Recientemente se mostró que esta condición da lugar a comportamientos físicamente inadecuados del pulso. Modelos con condiciones de frontera más sólidas existen para formaciones no-fracturadas pero no para fracturadas, para las cuales se emplea comúnmente el modelo tradicional, lo cual puede llevar a conclusiones erróneas. En este trabajo se presentan dos formulaciones para medios fracturados que están basadas en condiciones de frontera sólidas que especifican (i) la cantidad total de trazador inyectado, y (ii) el flujo de trazador en la frontera. Las nuevas formulaciones son comparadas con el modelo tradicional en términos de las diferencias en la curva de surgencia del trazador. Las discrepancias son importantes a números Peclet pequeños. Ellas son cuantificadas empleando (a) valores típicos para los parámetros involucrados en los modelos, y (b) ajustando los tres modelos al mismo conjunto de datos de pruebas de trazadores y comparando el valor de los parámetros obtenidos. En el primer caso la diferencia encontrada es 25% y en el segundo de 1% a 10%. En general estas discrepancias son pequeñas, pero podrían ser significativas en algunos casos.

**Descriptores:** Condiciones de frontera; transporte de trazador; medios porosos; yacimientos fracturados.

PACS: 05.60.Cd

## 1. Introduction

In Geosciences, specifically in the study of aquifers, petroleum reservoirs and geothermal fields, inter-well tracer tests are used to determine subsurface flow communication channels, study contaminant behavior and estimate geological formation properties. In these tests, a tracer is introduced into the underground formation through an injection well, and its arrival at the surrounding observation wells is monitored [1,2]. The tracer breakthrough curve, *i.e.* tracer concentration as a function of time in the observation well, contains information about the characteristics of the porous media along the tracer flow path. By fitting appropriate tracer transport models to the breakthrough data, properties such as porosity, dispersion coefficient, formation thickness, block size or fracture width can be estimated.

During the past six decades, many analytical models on this subject have been developed for divers cases and conditions; however, there are some basic assumptions proposed in deriving these models, which in reality lack a solid physi-

cal basis. This is the particular case of certain boundary and initial conditions. Boundary conditions in tracer transport models are regularly set by the tracer concentration (Dirichlet or type-one conditions) or the tracer flow (Cauchy or type-three conditions) [2-4]. The selection of appropriate boundary conditions in field tests or laboratory experiments has been the subject of many papers [see for example Refs. 5 to 8], since actual boundary conditions are in reality not well known. Author discussions on this subject gave rise to the unnecessary and confusing definitions of the so called “resident” and “flowing” tracer concentration [6]. More recent work on boundary conditions in tracer transport laboratory experiments concentrate on the effect of the mixing tanks located prior and after the porous column [7,8]. In a field tracer test, fluid mixing occurs inside the injection or production pipeline transporting the fluids between the surface and the underground formation.

A boundary condition commonly used in analytical models for instantaneous or finite-step tracer injection in porous media describes the tracer concentration at the injection bor-

der as a discontinuous function of time, specifically as a Dirac delta or a finite-step function [4,9-11]. It has been shown by Coronado *et al.* [12], that this condition gives place to physically improper mass conservation and pulse behavior due to the presence of strong, spurious dispersive backward flows at the tracer injection entrance border. The subject has been known to some extent to various researchers [13] who used the “resident” and “flowing” concentration concepts, and a few practitioners, but it was not properly documented until the paper in Ref. 12. Nevertheless, models based on this type of questionable boundary conditions remain in use [1,14-16], and an estimate of the possible errors incurred in is therefore desirable.

For non-fractured media there are tracer pulse transport models available that employ physically rigorous boundary conditions [see for example Refs. 3, 4, 7, and 17]. One of these models, which sets conditions from the total injected tracer mass [3] instead of the improper boundary condition [10], gives differences in the breakthrough curve that can be quantified at 30% or even larger for a Peclet numbers smaller than five [18]. In the case of analytical models for fractured media, the situation is different. Although several deterministic models for tracer pulse transport in diverse situations have been developed in the past, they all make use of the above mentioned controversial boundary condition [see for example Refs. 9, 11 and the review in Ref. 19] or the fully equivalent [12] time derivative technique [20,21] and superposition principle [16].

In order to provide models with physically solid boundary conditions, the original formulation of Sudicky and Frind for continuous tracer injection [22] and Maloszewski and Zuber for pulse injection [23] have been considered in this paper and adequately modified. Two new formulations have been obtained by introducing conditions (i) on the injection flow, and (ii) on the total injected tracer mass. In Sec. 2 of this paper, the boundary conditions and the models are presented. Model differences are quantified in terms of the breakthrough curves in Sec. 3 by providing typical model parameter values, and in Sec. 4 by fitting the models to published data obtained from tracer tests in three different field sites. Conclusions are drawn in Sec. 5. Mathematical details of calculations and mass balance are presented in the Appendices.

### 2. Boundary conditions and models

The presence of a network of well interconnected pathways in fractured formations can lead to regions of highly mobile fluid along the fractures (which can lead to large Peclet numbers), and very slowly moving fluid regions inside the porous rock matrix. To deal with the boundary condition problem, we consider the traditional two-dimensional system,  $(x, z)$ , composed of a series of parallel fractures separated by a slab of porous matrix [9,22,23], as schematically shown in Fig. 1. The standard double population approach is used to model tracer transport in the fracture network [mobile population 1,  $C_1(x, t)$ ], and in the porous matrix region [stagnant popula-

tion 2,  $C_2(x, z, t)$ ]. In this approach, both populations form a continuum in the entire space which represent the fracture system and the porous rock system, respectively. The mobile population is coupled to the stagnant population via transversal tracer diffusion from the fractures to the rock matrix. The total amount of tracer going into the matrix due to diffusion is artificially introduced into the mobile population as a sink smeared over the entire fracture volume. The resulting tracer conservation equations are [9,23,24]:

$$\frac{\partial C_1}{\partial t} + u \frac{\partial C_1}{\partial x} - D_1 \frac{\partial^2 C_1}{\partial x^2} - \frac{\phi_2 D_2}{w} \frac{\partial C_2}{\partial z} \Big|_{z=w} = 0 \quad (1)$$

$$\frac{\partial C_2}{\partial t} - \frac{D_2}{R_a} \frac{\partial^2 C_2}{\partial z^2} = 0. \quad (2)$$

Here subscripts 1 and 2 in dispersion/diffusion coefficients  $D$  and porosity  $\phi$  refer to the region describing the fracture or the matrix, respectively;  $u$  is a constant tracer velocity along the fractures;  $2w$  is the effective fracture width;  $R_a$  is a retardation factor due to stagnant tracer adsorption/desorption on the rock. Equation (1) is a modified advection-dispersion equation for fractures, while Eq. (2) is a diffusion equation for the porous rock.

The boundary and initial conditions for the stagnant population are the same as the traditional model and the two new models to be discussed here, namely:

$$C_2(x, z, t = 0) = 0 \quad (3)$$

$$C_2(x, z = w, t > 0) = C_1 \quad (4)$$

$$\partial C_2(x, z = E/2, t > 0) / \partial z = 0, \quad (5)$$

where  $E$  is the transversal matrix block size. Condition (5) establishes the absence of transverse flow communication between parallel fractures. The conditions for the mobile population are different in each of the three models to be presented here. The traditional condition set is [9]

$$C_1(x > 0, t = 0) = 0 \quad (6)$$

$$C_1(x = 0, t) = A\delta(t_+) \quad (7)$$

$$C_1(x \rightarrow \infty, t) = 0, \quad (8)$$

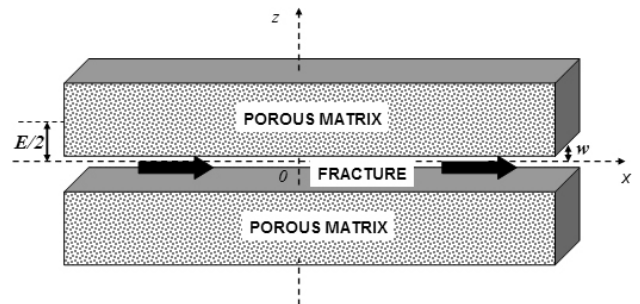


FIGURE 1. Schematic representation of a porous fractured medium in terms of fracture and porous matrix slabs.

where the Dirac delta  $\delta(t_+)$  means  $\delta(t - 0_+)$  and  $A$  is a constant to be related to the total tracer mass injected,  $M$ . Maloszewski and Zuber [9] give  $A = M/Q$ , with  $Q$  the volumetric flow rate of the injection fluid. This flow rate can be written as  $Q = u\phi_1 S$ , where  $u$  is the interstitial fluid velocity,  $S$  the flow total cross section and  $\phi_1 S$  the flow effective interstitial cross section [3]. Equation (7) displays the above physically improper boundary condition mentioned. The solution of Eqs. (1) to (8) in Laplace space given by Maloszewski and Zuber is [23]

$$\bar{C}_1^{(c)}(x_D, s_D) = \frac{M}{\phi_1 S L} \times \exp\left\{\frac{x_D P_e}{2} \left[1 - \sqrt{1 + 4\sigma_D/P_e}\right]\right\}, \quad (9)$$

where

$$\sigma_D(s_D) = s_D + \beta\sqrt{s_D} \tanh[\Theta\sqrt{s_D}], \quad (10)$$

and

$$x_D = x/L, \quad z_D = z/L, \quad t_D = tu/L, \quad (11)$$

$$P_e = \frac{uL}{D_1}, \quad \beta = \frac{\phi_2 L}{w} \sqrt{\frac{R_a D_2}{uL}},$$

$$\Theta = \sqrt{\frac{uLR_a}{D_2}} \left(\frac{E}{2L} - \frac{w}{L}\right) \quad (12)$$

Here  $L$  is a characteristic system length, such as the distance between wells. The Laplace variable  $s_D$  is dimensionless. The index  $(c)$  in  $\bar{C}_1^{(c)}$  means boundary conditions set on concentration. The expression in Eq. (9) is the same obtained in Ref. 21 by using the so called time derivative method. Maloszewski and Zuber [23] found an analytical expression in real space for the Laplace inverse of Eq. (9). This solution is given in terms of an integral that should be evaluated numerically.

The physical inconsistencies of model  $C_1^{(c)}(x, t)$  become apparent when analyzing the space dependence of the tracer pulse or evaluating the total tracer mass inside the system as a function of time,

$$m^{(c)}(t) = \int_0^\infty C_1^{(c)}(x, t) dx.$$

A constant or a temporarily increasing mass would be expected, as a result of the pulse inflow at  $x = 0$ . However, a quite different dynamic is found in reality, as described by Coronado *et al.* [12] for a non-fractured system (*i.e.*  $\beta = 0$ ). Here, the tracer pulse has an infinite starting mass and a permanent zero tracer concentration at  $x = 0$ , accordingly to condition (7). This last condition forces a strong positive concentration gradient to be formed at  $x = 0$ , which in turn generates a backward dispersion flow ( $-D_1 \partial C_1^{(c)} / \partial x$ ) at this point that actually transports tracer mass back outside the system. Therefore, the total mass is reduced continuously in time and asymptotically reaches the injected tracer mass. For a fractured system,  $\beta > 0$ , the pulse behavior is similar, but due to the porous matrix diffusive losses, the total tracer mass  $m^{(c)}(t)$  decreases continuously in time, as shown in Appendix A.

The two new formulations developed herein describe two common carrier fluid injection situations: (a) the tracer pulse is introduced in a short slug of carrier fluid (*fluid slug injection*), and (b) the tracer pulse is introduced in a continuous carrier fluid inflow (*continuous fluid injection*) [17]. In both cases, physically solid conditions are imposed. In the first case (a), we consider an infinite system and give the total tracer mass injected in  $x = 0$  at  $t = 0$  as a Dirac delta mass pulse. The initial and boundary conditions on  $C_1$  are therefore [3]

$$C_1(x, t = 0) = \frac{M}{S\phi_1} \delta(x), \quad (13)$$

$$C_i(|x| \rightarrow \infty, t) = 0. \quad (14)$$

After some algebraic manipulations (see Appendix B), the solution in Laplace space is obtained as

$$\bar{C}_1^{(M)}(x_D, s_D) = \begin{cases} \left(\frac{M}{\phi_1 S L}\right) \frac{\exp\left\{\frac{x_D P_e}{2} \left[1 - \sqrt{1 + 4\sigma_D/P_e}\right]\right\}}{\sqrt{1 + 4\sigma_D/P_e}} & x_D \geq 0 \\ \left(\frac{M}{\phi_1 S L}\right) \frac{\exp\left\{\frac{x_D P_e}{2} \left[1 + \sqrt{1 + 4\sigma_D/P_e}\right]\right\}}{\sqrt{1 + 4\sigma_D/P_e}} & x_D < 0 \end{cases}. \quad (15)$$

The superscript (M) in  $\bar{C}_1^{(M)}$  refers to conditions set by the total injected tracer mass. Here, the total tracer mass inside the system is

$$m^{(M)}(t) = \int_{-\infty}^\infty C_1^{(M)}(x, t) dx.$$

For  $\beta = 0$ , the total mass is constant and equal to the injected tracer mass,  $M$ , as expected. For  $\beta > 0$ , the mass  $m^{(M)}$  decreases continuously in time due to the matrix diffusive losses, as shown in Appendix A.

The second case (*continuous fluid injection*) is obtained by setting the tracer pulse as a flow pulse at the injection border at  $x = 0$ . A semi-infinite system with the following initial and boundary conditions is considered:

$$C_1(x, t = 0) = 0, \tag{16}$$

$$J_1(0, t) = \frac{M}{\phi_1 S} \delta(t_+), \tag{17}$$

$$C_1(x \rightarrow \infty, t) = 0. \tag{18}$$

The solution in Laplace space (see Appendix C) is

$$\begin{aligned} \bar{C}_1^{(J)}(x_D, s_D) \\ = \frac{2M}{\phi_1 SL} \frac{\exp\left\{\frac{x_D Pe}{2} \left[1 - \sqrt{1 + 4\sigma_D/Pe}\right]\right\}}{1 + \sqrt{1 + 4\sigma_D/Pe}}. \end{aligned} \tag{19}$$

The superscript (J) in  $\bar{C}_1^{(J)}$  means conditions set by the tracer flow. The total system tracer mass,

$$m^{(J)}(t) = \int_0^\infty C_1^{(J)}(x, t) dx,$$

behaves exactly as  $m^{(M)}(t)$  does (Appendix A).

The Laplace inversion of Eqs. (15) and (19) will be performed numerically. To compare these solutions with the traditional Maloszewski and Zuber case we calculate the Laplace inversion of Eq. (9) also numerically.

The free parameters involved in the three models, Eqs. (9), (15) and (19), are  $Pe$ ,  $\beta$  and  $\Theta$ , as defined in Eq. (12). In tracer breakthrough curve analysis, the variable  $x_D$  can be used as a fitting parameter,  $x$  being the real underground transit length. The scale parameter,  $C_R = M/\phi_1 SL$ , works as an additional linear model free parameter. The  $\beta$  value describes the importance of the tracer diffusion into the rock in relation to tracer flow along the fracture. As previously mentioned, the non-fractured case is recovered when no diffusion from the fracture to the matrix is present, *i.e.*  $\beta = 0$ . The parameter  $\Theta$  is linked to the presence of multiple interacting parallel fractures. The model for a single fracture is recovered when  $\Theta$  is large (*i.e.*  $E \rightarrow \infty$ ). For  $\Theta \geq 2$ , it is true that  $\tanh \Theta \approx 1$ , and the multiple fracture effect is negligible. This case is also known as a short-term experiment, since the transit time is sufficiently short to prevent the tracer from diffusing deep enough into the rock matrix in order to notice the presence of adjacent fractures [11,24]. In this case, Eq. (10) translates into

$$\sigma_D(s) = s_D + \beta\sqrt{s_D}, \tag{20}$$

and the parameter  $\Theta$  disappears from the models. There are four free parameters left in the models, namely  $Pe$ ,  $\beta$ ,  $x_D$  and the scale parameter,  $C_R$ .

### 3. Model comparison by specifying typical model parameter values

The new models described by Eqs. (15) and (19) are compared with the traditional model in Eq. (9) using De Hoog's algorithm for numerical Laplace inversion [25]. For this purpose, the behavior of the dimensionless tracer concentrations defined by  $C_D^{(i)}(x_D, t_D) = C_1^{(i)}(x_D, t_D)/C_R$  is analyzed. Here, index  $i$  in  $C_D^{(i)}$  is valid for  $c$ ,  $M$  or  $J$ . The approximation in Eq. (20) will be used when comparing models. A representative value for  $Pe$  is 10; nevertheless, in fractured systems, larger values of  $Pe$  could be expected due to the relatively high speed flows developed. On the other hand, the parameter  $\beta = \phi_2(L/w)\sqrt{(R_a/Pe)(D_2/D_1)}$  can take a broad range of values; however, to estimate it, we consider the case when  $\phi_2 \approx 0.1$ ,  $L/w \approx 10^6$ ,  $R_a = 1$  and  $D_2/D_1 \approx [10^{-11} - 10^{-7}]$ . It follows that  $\beta \approx [0.1 - 10]$ . Figure 2 presents  $C_D^{(i)}$  as a function of  $x_D$  for (a)  $t_D = 0.1$  and (b)  $t_D = 1$ , with  $Pe=10$  and  $\beta=0.5$ . Curves  $C_D^{(M)}$  and  $C_D^{(J)}$  describe a standard inlet pulse at  $x_D=0$  arriving from the left, while  $C_D^{(c)}$  shows an anomalous behavior, as described previously. The condition  $C_D^{(c)}(x_D = 0, t_D > 0_+) = 0$  forces the  $C_1^{(c)}$  pulse to leave the injection site ( $x_D = 0$ ) earlier than  $C_1^{(J)}$  and  $C_1^{(M)}$  pulses do. For longer times, the three curves become similar. In Fig. 3, tracer breakthrough curves  $C_D^{(i)}(t_D)$  are shown for (a)  $Pe = 5$  and (b)  $Pe=50$ , with  $x_D = 1$ , and  $\beta=3$ . It can be observed that large model differences appear for small  $Pe$  values. The model differences can be quantified by evaluating

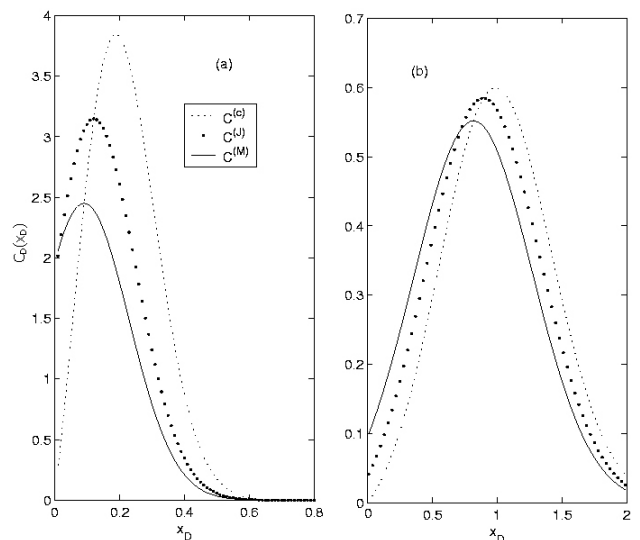


FIGURE 2. Normalized tracer concentration as function of space for (a)  $t_D = 0.1$  and (b)  $t_D = 1$ , with  $Pe = 10$  and  $\beta = 0.5$  in the three models. The curves describe the behavior of a pulse appearing in  $x_D = 0$  at  $t_D = 0$  and moving to the right. Observe that  $C_1^{(c)}(t_D > 0) = 0$  holds, and that curves get similar to each other at large times.

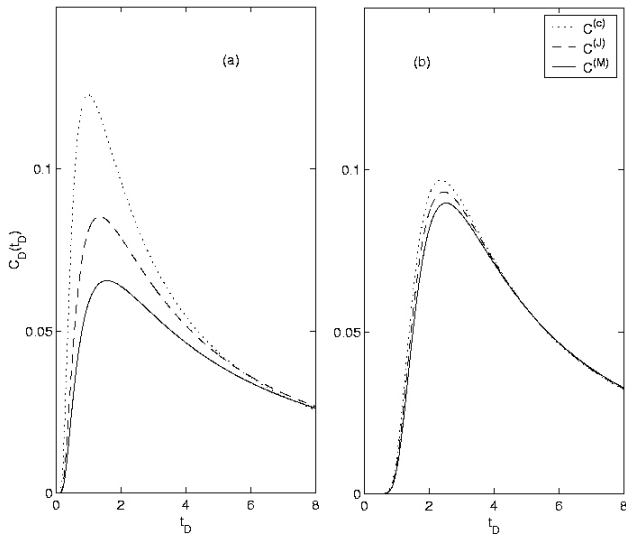


FIGURE 3. Dependence on the Peclet number. Breakthrough curves for (a)  $Pe=5$  and (b)  $Pe=50$  with  $x_D=1$  and  $\beta=3$ .

$$\Delta C^{(i)} \equiv \int_0^\infty |C_D^{(c)} - C_D^{(i)}| dt_D / \int_0^\infty C_D^{(c)} dt_D. \quad (21)$$

For  $Pe=10$ ,  $x_D=1$  and  $\beta=3$ , it follows that  $\Delta C^{(J)} = 8.3\%$  and  $\Delta C^{(M)} = 13.0\%$ . These discrepancies increase by reducing the matrix effects. Thus, setting  $\beta$  to 0.5, this yields  $\Delta C^{(J)} = 14.4\%$  and  $\Delta C^{(M)} = 26.0\%$ . Also, by reducing  $Pe$  to 5, while keeping  $x_D=1$  and  $\beta=3$ , the differences increase to  $\Delta C^{(J)} = 12.3\%$  and  $\Delta C^{(M)} = 20.7\%$ .

#### 4. Model comparison by field data fitting

To obtain a meaningful quantification of model differences, we make use of real data from field tracer tests in fractured formations. The three models are fitted to the same data set to determine discrepancies in the resulting free parameter values. This will provide a good estimate of the relative error when selecting a certain boundary condition over another. The use of a one-dimensional model to describe real 3D tracer transport can be justified by only taking into consideration the space formed by the communication channel between the injector and a single production well. We assume the flow along the channel path is approximately uniform. Here  $M$  means the total tracer mass fraction introduced in the communication channel, and  $S$  its average cross section.

The three models depend on the parameters  $x_D$ ,  $Pe$  and  $\beta$ , plus the scaling factor  $C_R$ . In order to apply the models to real field data, a characteristic time,  $t_c$ , is introduced together with the new dimensionless variable  $t_d = t/t_c$ . This new variable is necessary because  $t_D$  is inadequate since it involves  $u$ , which is part of the fitting parameters. The characteristic time might be, for example, the average tracer transit time or any other time such as the peak concentration transit time or the first arrival time. The transformation  $t_D \rightarrow t_d \xi$

should be carried out, where  $\xi = ut_c/L$ . In Laplace space this change implies  $\overline{C}_1^{(i)}(s_D) \rightarrow \xi \overline{C}_1^{(i)}(s_D/\xi)$ . The structure of  $\overline{C}_1^{(i)}$  in terms of the variable  $s_D$  remains exactly the same if new fitting parameters are defined as  $\alpha_1 = x_D/\xi$ ,  $\alpha_2 = \xi Pe$ ,  $\alpha_3 = \sqrt{\xi} \beta$  together with  $\alpha_4 = \xi C_R$ . It is noteworthy that parameter  $\alpha_1$  is proportional to the parameter  $t_0 = x/u$  introduced by Maloszewski and Zuber [9,11,24] (i.e.  $t_0 = \alpha_1 t_c$ ), and parameter  $\alpha_3$  to their parameter  $a$ .

The fitting procedure starts with the selection of  $t_c$  in order to normalize time. Later an objective function is defined, here a non-weighted sum of the square of the errors, and then an optimization method is selected, here the Levenberg-Marquardt and the Broyden-Fletcher-Goldfarb-Shanno methods [26]. In applying the optimization process, some appropriate initial parameter values should be provided and a sensitivity analysis should be performed in order to study solution uniqueness [27]. The parameter range we consider in our analysis is  $\alpha_1 \in [0.1, 2]$ ,  $\alpha_2 \in [5, 200]$ , and  $\alpha_3 \in [0, 4]$ . The previously mentioned De Hoog's algorithm is used to obtain the inverse Laplace transform numerically. Once the optimized parameters  $\{\alpha_1, \alpha_2, \alpha_3, \alpha_4\}$  are determined the original fitting parameters can be obtained using the  $\alpha_i$  definition. For instance, if  $x_D = 1$  is taken, then  $\xi$  can be calculated from  $\xi = x_D/\alpha_1$ , and then  $Pe$ ,  $\beta$  and  $C_R$  can be evaluated using the expression for  $\alpha_2$ ,  $\alpha_3$  and  $\alpha_4$ , respectively. From these quantities, some properties of the system can be estimated (see for example Ref. 11). From  $C_R$  for instance, the average flow cross section,  $S$ , can be obtained.

Three different published tracer tests performed on fractured formations are analyzed in the next section. Each of these applications has a different origin and different characteristics. The three cases are: an experimental aquifer with a transit length  $L=11.8$  m, a geothermal field with  $L=210$  m, and an oil field with  $L=2182$  m. The injection situation in the first case corresponds to a *fluid slug injection*  $C_1^{(M)}$ , while other two cases corresponds to *continuous fluid injection*, i.e.  $C_1^{(J)}$ . The three models were fitted to all three field cases.

##### 4.1. Aquifer in an experimental field in Ontario

Data from a tracer test performed in an experimental field site located in west of Ontario and developed to study fluid flow in fractured porous media are considered [28]. The test was carried out in a single fracture layer saturated with water. In the experiment, a 0.17 liter pulse of a concentrated fluorescent dye (at 1000 mg/l) was injected in well 1 and its arrival at the surrounding wells monitored. The specific data used in this paper concern the tracer response at well 19 (see data points in Fig. 4). The value used for the characteristic time is  $t_c = 129h$ . The initial parameter values employed in the fitting procedure are  $\alpha_1 = 0.5$ ,  $\alpha_2 = 0.25$  and  $\alpha_3 = 0.06$ . No initial value is required for  $C_R$ , since it is a linear multiplicative parameter. The solution with the lowest objective function value for each model is:

$$C^{(c)} - \text{Model} : \quad \alpha_1 = 0.431, \\ \alpha_2 = 161.7, \quad \alpha_3 = 1.179 \quad (22)$$

$$C^{(M)} - \text{Model} : \quad \alpha_1 = 0.419, \\ \alpha_2 = 166.7, \quad \alpha_3 = 1.180 \quad (23)$$

$$C^{(J)} - \text{Model} : \quad \alpha_1 = 0.425, \\ \alpha_2 = 163.1, \quad \alpha_3 = 1.179. \quad (24)$$

The same value  $\alpha_4 = 62.79 \mu\text{g/l}$  is obtained in all three cases. In Fig. 4, a plot of the fitting curves is displayed (the value  $C_0 = 15 \text{ mg/l}$  given by Lapcevic *et al.* [27] was used). All three models give the same curve and therefore they appear overlap. The largest parameter difference found in Eqs. (22) to (24), relative to  $C^{(c)}$ , is around 1.5% for  $C^{(J)}$  and 3.1% for  $C^{(M)}$ . By setting  $x_D = 1$  and employing the values in Eq. (22), it follows that that  $\xi = 2.39$ ,  $Pe=69.7$  and  $\beta=0.76$ . The discrepancies found between the models are small in this case, probably due to the large  $Pe$  value.

#### 4.2. Wairakei geothermal field

We analyze one of the two tracer tests performed in the Wairakei reservoir to determine underground communication channels [29]. This field is a major liquid dominated geothermal fractured reservoir located in New Zealand. In the test that interests us here, a  $155 \text{ GBq}$  pulse of the radioactive Iodine-131 in well WK107 at 334 m a depth of was introduced, and its arrival in well WK24 located at a distance of 210 m from injector is analyzed. We have selected this well pair because the tracer response curve has relatively low data dispersion, which could be an indication of a simple communication channel. The characteristic time  $t_c = 0.214$  days (breakthrough time) is chosen. As in the previous case, the three models under consideration are fitted to the same data set in order to determine  $\alpha_1, \alpha_2, \alpha_3$  and  $C_R$ . The initial parameter values employed are  $\alpha_1 = 1, \alpha_2 = 20, \alpha_3 = 2$ . The solution obtained is:

$$C^{(c)} - \text{Model} : \quad \alpha_1 = 1.325, \\ \alpha_2 = 88.76, \quad \alpha_3 = 1.804 \quad (25)$$

$$C^{(M)} - \text{Model} : \quad \alpha_1 = 1.302, \\ \alpha_2 = 90.42, \quad \alpha_3 = 1.805 \quad (26)$$

$$C^{(J)} - \text{Model} : \quad \alpha_1 = 1.314, \\ \alpha_2 = 89.06, \quad \alpha_3 = 1.804. \quad (27)$$

The same value,  $C_R = 7.303 \times 10^4 \text{ Bq}$ , is obtained in the three cases (the volume of the analysis sample was not specified). A plot of the original data and the fitting curves is presented in Fig. 5. As in the previous case, the three models yield overlapping curves. Sensitivity analysis indicates the presence of a single global minimum around the values in

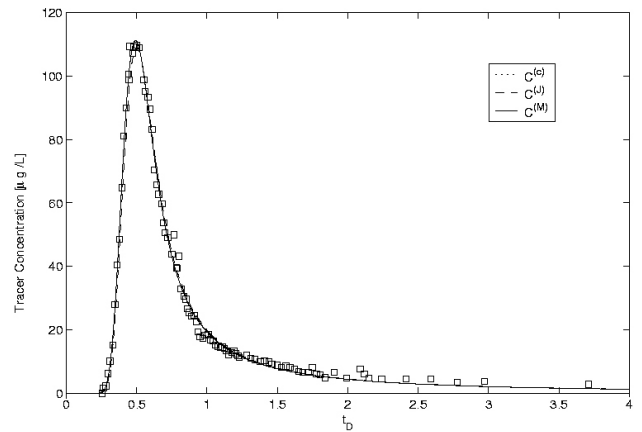


FIGURE 4. Breakthrough data (squares) for the tracer test in an aquifer near Ontario and model curves resulting from data fitting. The three models  $C_1^{(c)}, C_1^{(J)}$ , and  $C_1^{(M)}$  give overlapping curves.

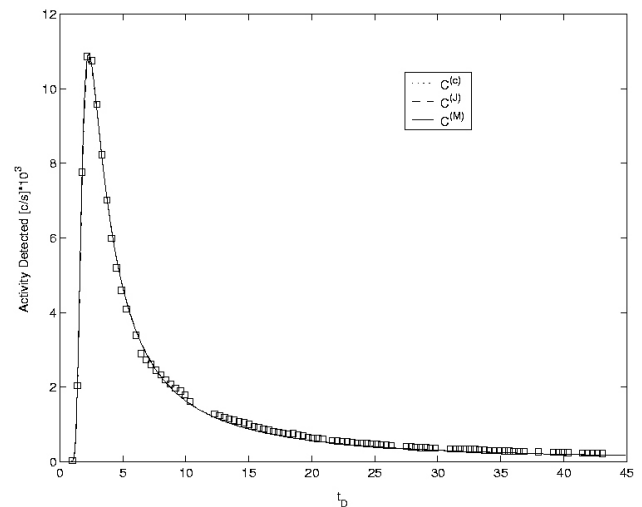


FIGURE 5. Breakthrough data (squares) for the tracer test in the Wairakei geothermal field together with curves obtained from model fitting. The three models  $C_1^{(c)}, C_1^{(J)}$ , and  $C_1^{(M)}$  give almost overlapping curves.

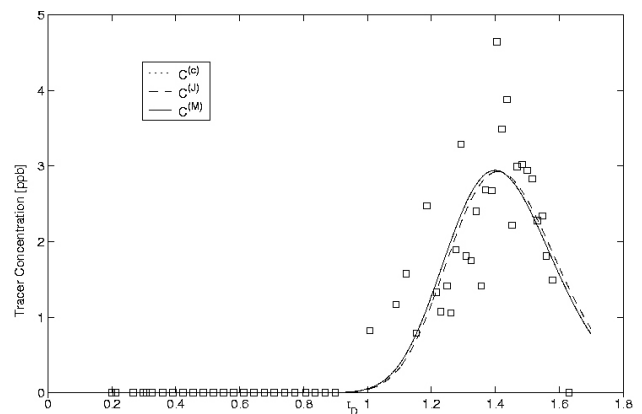


FIGURE 6. Breakthrough data (squares) for the tracer test in the Chiapas-Tabasco Basin oil field together with curves obtained from model fitting. Here dots are overlapped by the solid line. The large data dispersion is probably due to multiphase fluid and formation complexities present.

Eqs. (25) to (27). The corresponding parameter differences relative to model  $C^{(c)}$  are less than 1% for  $C^{(J)}$  and less than 2% for  $C^{(M)}$ . As in the previous case, the model discrepancies are very small. By setting  $x_D = 1$  and using Eq. (27), it turns out that  $\xi = 0.761$ ,  $Pe=117.0$  and  $\beta=2.07$ . Again, the modest model discrepancies can be attributed to the very large  $Pe$  value involved.

### 4.3. Chiapas-Tabasco Oil Basin

A tracer test was carried out on a fractured oil field in the Chiapas-Tabasco Basin in Mexico in order to determine interwell connectivity [30]. A short pulse of 20.25 Kg Perfluoromethylcyclohexane (PMCH) tracer was injected in the permanent injector well 12, and its arrival at different production wells is analyzed. Here, the data obtained from production well 5 located 2182 m away from the injector at a depth of nearly 6000 m is analyzed. As in the two previous sections, breakthrough data are fitted by the three models under consideration. Here,  $t_c = 444.1$  d and the initial parameters  $\alpha_1 = 1$ ,  $\alpha_2 = 10$  and  $\alpha_3 = 1$  are employed. The solution obtained is:

$$C^{(c)} - \text{Model} : \quad \alpha_1 = 1.432, \quad \alpha_2 = 90.41, \\ \alpha_3 = 1 \times 10^{-5}, \quad C_R = 1272.0\text{ppt} \quad (28)$$

$$C^{(M)} - \text{Model} : \quad \alpha_1 = 1.409, \quad \alpha_2 = 97.01, \\ \alpha_3 = 1 \times 10^{-8}, \quad C_R = 1249.9\text{ppt} \quad (29)$$

$$C^{(J)} - \text{Model} : \quad \alpha_1 = 1.419, \quad \alpha_2 = 98.15, \\ \alpha_3 = 2 \times 10^{-7}, \quad 2C_R = 2479.6\text{ppt} \quad (30)$$

The fitting curves are shown in Fig. 6. The parameter differences among models relative to  $C^{(c)}$  are less than 9% for  $C^{(J)}$  and less than 8% for  $C^{(M)}$ . For  $x_D = 1$ , it follows from Eq. (30), that  $\xi = 0.705$ ,  $Pe=139.2$  and  $\beta=2.38 \times 10^{-7}$ . Although the tracer breakthrough data shows high dispersion (see Fig. 6), the models give very similar parameter values. This result might be attributed to the large  $Pe$  value, as in the previous two cases. The value  $\beta \approx 0$  could indicate a poor porous matrix participation in the system fluid flow.

## 5. Summary and conclusions

This paper concerns a controversial boundary condition frequently employed in models for tracer transport in fractured underground formations. The effects of using this condition have been previously analyzed for non-fractured media, but not for fractured media. In the first case, tracer breakthrough curve differences of 30% have been reported in comparison to models with physically sounder boundary conditions.

All available deterministic analytical models for tracer transport in fracture formations make use of the debatable condition. In this paper two new one-dimensional formulations that make use of physically more rigorous boundary conditions have been developed, which apply in different circumstances. These new models impose conditions on

- (i) the total tracer injected mass and
- (ii) the tracer flow at the injection border respectively.

The solutions are found in Laplace space and the inversion is made numerically using De Hoog's algorithm. Differences from the traditional model are evaluated in terms of tracer breakthrough curves by using typical values for the two free model parameters involved, which are the Peclet number ( $Pe$ ) and the fracture-matrix coupling parameter ( $\beta$ ). For  $Pe=10$  and  $\beta=3$ , the models yield discrepancies smaller than 13%. Differences get larger when reducing  $Pe$  or  $\beta$ . Thus, for  $Pe=10$  and  $\beta=0.5$ , these discrepancies increase to 26%, and for  $Pe=5$ ,  $\beta=3$ , they become 21%. Real reservoir tracer test data were also employed to determine fitting parameter differences resulting from the models. Three separate data sets from dissimilar geophysical applications and different interwell distances ( $L$ ) have been considered. The cases were an aquifer with  $L \approx 12$ m, a geothermal field with  $L \approx 210$  m, and an oil field with  $L \approx 2200$  m. Model differences found from the tracer breakthrough data matching are small; they are less than or similar to 3% in the two first cases and less than 9% in the third case. The origin of these small differences seems to be based on the large Peclet numbers appearing (70, 117 and 139). Other tracer field data were examined, but no significantly smaller value of  $Pe$  was found. To obtain smaller Peclet numbers once large fluid flows are present, very intensive fluid mixing due to the fracture network would be required. We can conclude that, in general, in fractured formations the traditional and the two new boundary conditions yield relatively similar results regarding the breakthrough curve. Larger data precision in field tracer tests would be required to observe significant discrepancies. However, regarding space dependence and mass conservation, the models contain relevant differences. The traditional model shows physical inconsistencies, particularly at short transit times.

## Appendix A: The tracer mass

### A-1. The total injected tracer mass

The total amount of tracer injected in the system can be evaluated using the solutions in Laplace space by noticing [12]

$$M_{inj} = \phi_1 S \int_0^\infty J_1(x=0, t) dt = \phi_1 S \int_0^\infty \left\{ u C_1(x=0, t) - D_1 \left[ \frac{\partial C_1(x, t)}{\partial x} \right]_{x=0} \right\} dt = \phi_1 S u \left[ \int_0^\infty C_1(x, t) e^{-st} dt \right]_{s=0, x=0} - \phi_1 S D_1 \left\{ \frac{\partial}{\partial x} \left[ \int_0^\infty C_1(x, t) e^{-st} dt \right] \right\}_{s=0, x=0} = \phi_1 S u \overline{C}_1(x=0, s=0) - \phi_1 S D_1 \left. \frac{\partial \overline{C}_1(x, s)}{\partial x} \right|_{s=0, x=0}. \quad (A.1)$$

The first term on the RHS gives the tracer inflow due to the convection process and the second term provides the net inflow due to dispersion. In terms of the dimensionless variables defined in Eqs. (11) and (12), and using  $\overline{C}_1(s_D) = (u/L)\overline{C}_1(s)$  with  $s_D = sL/u$ , this yields

$$M_{inj} = \phi_1 S L \overline{C}_1(x_D=0, s_D=0) - \frac{\phi_1 S D_1}{u} \left. \frac{\partial \overline{C}_1(x, s)}{\partial x_D} \right|_{s_D=0, x_D=0}. \quad (A.2)$$

For the model  $C_1^{(c)}$ , after substitution of Eq. (9), it follows that the dispersion term vanishes and  $\overline{C}_1^{(c)}(x=0, s=0) = M/\phi_1 S L$ ; the results give  $M_{inj} = M$ , as expected. The same results follow for models  $C_1^{(M)}$  and  $C_1^{(J)}$  using Eqs. (15) and (19), respectively.

**A-2. The total tracer mass inside the system**

The total tracer mass inside the system for  $C_1^{(c)}$  and  $C_1^{(J)}$  is

$$m(t) = \phi_1 S \int_0^\infty C(x, t) dx. \quad (A.3)$$

The Laplace transform of Eq. (A.3) in terms of  $t_D = tu/L$  and  $s_D = sL/u$  yields

$$\overline{m}(s_D) = \phi_1 S L \int_0^\infty \overline{C}(x_D, s_D) dx_D. \quad (A.4)$$

Thus, the expressions for the tracer concentration in Laplace space  $\overline{C}_1$  can be employed to evaluate  $\overline{m}(s_D)$ . The expression for  $\overline{C}_1^{(c)}$  and  $\overline{C}_1^{(J)}$  has the form  $\Lambda(s) \exp[x_D \lambda(s)]$ ; therefore, the integral in Eq.(A.4) can be. It follows that

$$\overline{m}(s_D) = - \frac{\phi_1 S L \Lambda(s)}{\lambda(s)}. \quad (A.5)$$

By substituting expression (9) and (19), we get

$$\overline{m}^{(c)}(s_D) = \frac{M}{\frac{Pe}{2} [\sqrt{1 + 4\sigma_D/Pe} - 1]}, \quad (A.6)$$

and

$$\overline{m}^{(J)}(s_D) = \frac{2M}{\frac{Pe}{2} [(1 + 4\sigma_D/Pe) - 1]} = M \left( \frac{1}{\sigma_D} \right). \quad (A.7)$$

---

For  $C_1^{(M)}$ , the total system mass is given by

$$\overline{m}^{(M)}(s_D) = \phi_1 S L \times \left[ \int_{-\infty}^0 \overline{C}(x_D, s_D) dx_D + \int_0^\infty \overline{C}(x_D, s_D) dx_D \right]. \quad (A.8)$$

Substituting Eq. (15) into Eq. (A.8) yields the same result that  $\overline{m}^{(J)}(s_D)$  does, namely

$$\overline{m}^{(M)}(s_D) = M \left( \frac{1}{\sigma_D} \right). \quad (A.9)$$

It should be noticed that, for  $\beta = 0$  (no diffusion losses),  $\sigma_D(s) = s_D$  follows, and the inverse Laplace transform of  $\overline{m}^{(M)}(s_D)$  and  $\overline{m}^{(J)}(s_D)$  yields  $m(t) = M$ . Therefore, the total tracer mass inside the system is constant and equal to the total injected mass. This simple result does not hold for  $m^{(c)}(t)$ .

The general case with  $\beta > 0$  shows the presence of tracer losses due to diffusion into the porous matrix; therefore  $m^{(J)}(t) [= m^{(M)}(t)]$  is no longer a constant, but is reduced in time. In Fig. 7, two plots of  $m(t)/M$  are shown, in (a) for  $\beta = 0$  and in (b) for  $\beta = 0.5$ . In both cases,  $Pe=10$  was taken. Here, the improper behavior of  $m^{(c)}(t)$  is apparent, since it is infinite at the initial time, while  $m^{(J)}$  correctly yields  $m^{(J)}(t=0)/M = 1$ .

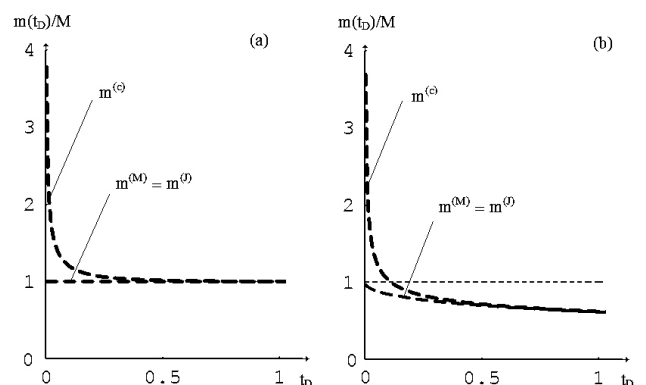


FIGURE 7. Total tracer mass inside the system accordingly to the three models, in (a) for  $\beta = 0$ , and in (b) for  $\beta = 0.5$ . In both plots  $Pe=10$  was set.

**Appendix B: Solution in Laplace space of the  $C^{(M)}$ -Model**

In this section, the solution in Laplace space of Eqs. (1) and (2) subject to conditions in Eqs. (3) to (5), (13) and (14) is presented. The Laplace transform of Eq. (2) together with initial condition (3) yields

$$s\overline{C_2}(x, z, s) - \frac{D_2}{R_a} \frac{\partial^2 \overline{C_2}(x, z, s)}{\partial z^2} = 0. \tag{B.1}$$

By seeking solutions of the type  $\overline{C_2} \propto \exp(z\gamma)$  it follows that

$$\overline{C_2}(x, z, s) = Z_+(x, s)e^{\gamma_+z} + Z_-(x, s)e^{\gamma_-z}, \tag{B.2}$$

where  $Z_+$  and  $Z_-$  are functions to be determined and

$$\gamma_{\pm} = \pm\sqrt{sR_a/D_2}. \tag{B.3}$$

The Laplace transform of boundary condition (5), which establishes the presence of multiple parallel fractures, gives

$$Z_-(x, s) = Z_+(x, s)e^{(\gamma_+ - \gamma_-)E/2}, \tag{B.4}$$

where  $\gamma_+/\gamma_- = -1$  was set. Boundary condition (3b) gives a relationship between  $\overline{C_2}$  and  $\overline{C_1}$ , namely

$$\begin{aligned} \overline{C_2}(x, z, s) &= \overline{C_1}(x, s)e^{\gamma_+(z-w)} \\ &\times \left[ \frac{1 + e^{(\gamma_+ - \gamma_-)(E/2 - z)}}{1 + e^{(\gamma_+ - \gamma_-)(E/2 - w)}} \right]. \end{aligned} \tag{B.5}$$

This expression makes it possible to find  $\overline{C_2}$  once the function  $\overline{C_1}$  is known. The Laplace transform of Eq. (1) yields

$$\begin{aligned} s\overline{C_1}(x, s) + u \frac{\partial \overline{C_1}(x, s)}{\partial x} - D_1 \frac{\partial^2 \overline{C_1}(x, s)}{\partial x^2} \\ - \left. \frac{\phi_2 D_2}{w} \frac{\partial \overline{C_2}(x, z, s)}{\partial z} \right|_{z=w} = C_1(x, t = 0); \end{aligned} \tag{B.6}$$

after the substitution of expression (B.5), the fourth term on the LHS becomes

$$\begin{aligned} \left. \frac{\phi_2 D_2}{w} \frac{\partial \overline{C_2}(x, z, s)}{\partial z} \right|_{z=w} &\rightarrow -\overline{C_1}(x, s) \frac{\phi_2 D_2 \gamma_+}{w} \\ &\times \tanh \left[ \frac{(\gamma_+ - \gamma_-)(E/2 - w)}{2} \right], \end{aligned} \tag{B.7}$$

where  $\tanh(y) = (e^{2y} - 1)/(e^{2y} + 1)$  was used. By using (B.3) and defining

$$\sigma(s) = s + \sqrt{s} \frac{\phi_2 \sqrt{D_2 R_a}}{w} \tanh \left[ \sqrt{\frac{s R_a}{D_2}} (E/2 - w) \right], \tag{B.8}$$

equation (B.6) translates into

$$\begin{aligned} \sigma(s)\overline{C_1}(x, s) + u \frac{\partial \overline{C_1}(x, s)}{\partial x} - D_1 \frac{\partial^2 \overline{C_1}(x, s)}{\partial x^2} \\ = C_1(x, t = 0). \end{aligned} \tag{B.9}$$

This last equation for  $\overline{C_1}(x, s)$  should be solved using the boundary conditions in Eqs. (13) and (14); after substitution of Eq. (13), it follows that

$$\begin{aligned} \sigma(s)\overline{C_1}(x, s) + u \frac{\partial \overline{C_1}(x, s)}{\partial x} - D_1 \frac{\partial^2 \overline{C_1}(x, s)}{\partial x^2} \\ = \frac{M}{S\phi_1} \delta(x). \end{aligned} \tag{B.10}$$

For  $x \neq 0$ , the RHS of Eq. (B.10) disappears and thus it has solutions to the exponential type  $\overline{C_1} \propto \exp(x\xi)$ . The characteristic equation for  $\xi$  yields

$$\xi_{\pm} = \frac{u}{2D_1} \left[ 1 \pm \sqrt{1 + 4D_1\sigma/u^2} \right]. \tag{31}$$

Here, it is true that  $\xi_+ > 0$  and  $\xi_- \leq 0$ . Therefore, for  $x \neq 0$ , the solution in Laplace space that satisfies conditions in Eq. (14) is

$$\begin{aligned} \overline{C_1}(x > 0, s) &= X(s)e^{\xi_-x} \\ \overline{C_1}(x < 0, s) &= X(s)e^{\xi_+x} \end{aligned} \tag{A.12}$$

where the continuity condition  $\overline{C_1}(x=0_+, s) = \overline{C_1}(x=0_-, s)$  was imposed. Here  $X(s)$  is a function to be determined through a flow continuity condition that can be derived from Eq. (B.10) by integrating it from  $x = -\varepsilon$  to  $x = \varepsilon$  and then taking  $\varepsilon \rightarrow 0$ . The first two terms on the LHS of the resulting equation vanish, leaving

$$-D_1 \left. \frac{\partial \overline{C_1}(x, s)}{\partial x} \right|_{0_-}^{0_+} = \frac{M}{S\phi_1}. \tag{A.13}$$

After substituting Eq. (B.12) in the last condition, it follows  $(\xi_+ - \xi_-)X(s) = M/D_1 S\phi_1$  and therefore for any  $x$  it follows

$$X(s) = \frac{M/S\phi u}{\sqrt{1 + 4\sigma D_1/u^2}}. \tag{A.14}$$

By employing the dimensionless variables and parameters defined in Eqs. (11) and (12), together with  $s_D = sL/u$  and  $\sigma_D = \sigma L/u$ , and realizing that  $\overline{C_1}(s_D) = (u/L)\overline{C_1}(s)$ , the solution shown in Eq. (15) follows.

**Appendix C: Solution in Laplace space of the  $C^{(J)}$ -Model**

In this case the boundary conditions are set in Eqs. (11). The whole formalism developed in Appendix B for  $\overline{C_2}(x, z, s)$  and  $\overline{C_1}(x, s)$  up to Eq. (B.9) is still valid; here however,  $C_1(x, t = 0) = 0$ , as established in Eq. (16). The solution for  $x \geq 0$  is therefore

$$\overline{C_1}(x, s) = Y(s)e^{\xi_-x}, \tag{C.1}$$

where the Laplace transformed condition of Eq. (18) was imposed, and  $Y(s)$  is an unknown function to be determined by the Laplace transform of Eq. (17). This gives the following condition on the flow:

$$\bar{J}_1(x=0, s) = (M/S\phi_1) \int_0^{\infty} \delta(t_+) e^{-st} dt = (M/S\phi_1). \quad (\text{C.2})$$

Using the Laplace transform of the flow

$$J_1(x=0, t) = uC_1(x=0, t) - D_1 [\partial C_1(x, t)/\partial x]_{x=0}$$

and Eq. (C.1), it follows that

$$uY(s) - D_1 \xi_- Y(s) = (M/S\phi_1), \quad (\text{C.3})$$

and therefore

$$Y(s) = \frac{2M/S\phi_1 u}{1 + \sqrt{1 + 4\sigma D_1/u^2}} \quad (\text{C.4})$$

By employing the dimensionless variables and parameters defined in Eqs. (11) and (12), together with  $s_D = sL/u$ ,  $\sigma_D = \sigma L/u$  and  $\bar{C}_1(s_D) = (u/L)\bar{C}_1(s)$ , the solution shown in Eq. (19) follows.

1. W. Käss, *Tracing Technique in Geohydrology* (A. Balkema, Rotterdam, 1998).
2. R.J. Charbeneau, *Groundwater Hydraulics and Pollutant Transport* (Prentice Hall, Upper Saddle River, NJ, 2000).
3. J. Bear, *Dynamics of Fluids in Porous Media* (Dover Publications, New York, 1972).
4. M. Th. Van Genuchten and W.J. Alves, *Analytical solutions on the one-dimensional convective-dispersive transport equation*. Technical Bulletin 1661, George E. Brown Jr. Salinity Laboratory, Unites States Department of Agriculture, Riverside, CA (1982). <http://ars.usda.gov/sp2UserFiles/Place/53102000/pdf-pubs/P0753.pdf>
5. N.D. Gershon and A. Nir, *Water Resour. Res.* **5** (1969) 830.
6. A. Kreft and A. Zuber, *Chem. Eng. Sci.* **33** (1978) 1471.
7. K.S. Novakowski, *Water Resour. Res.* **28** (1992) 2399.
8. R.C. Schwartz, K.J. McInnes, A.S.R. Juo, and L.P. Wilding, *Water Resour. Res.* **35** (1999) 671.
9. P. Maloszewski and A. Zuber, *J. Hydrology* **79** (1985) 333.
10. A. Lenda and A. Zuber, *Isotope Hydrology 1970* (IAEA, Vienna, 1970) p. 619.
11. P. Maloszewski and A. Zuber, *Water Resour. Res.* **26** (1990) 1517.
12. M. Coronado, J. Ramírez, and F. Samaniego, *Transp. Porous Med.* **54** (2004) 221.
13. V. Batu and M.T. van Genuchten, *Water Resour. Res.* **26** (1990) 339.
14. G. Mordis, *Water Resour. Res.* **38** (2002) 46; doi:10.1029/2001WR 001028.
15. A. Lange, J. Bouzian, and B. Bourbiaux, *Tracer-test simulation on discrete fracture network models for the characterization of fractured reservoirs*. SPE/EAGE Annual Conference, Madrid, Spain, 13-16 June 2005. Society of Petroleum Engineers library record # 94344, <http://www.spe.org>.
16. Ch. Shan and K. Pruess, *Water Resour. Res.* **41** (2005) W08502-1; doi:10.1029/2005WR004081.
17. M. Coronado and J. Ramírez, *Transp. Porous Med.* **60** (2005) 339.
18. M. Coronado, J. Ramírez-Sabag, O. Valdiviezo-Mijangos, and C. Somaruga, *Further considerations on the boundary conditions used in reservoir tracer test models: analysis of some field cases*. Submitted for publication.
19. P. Maloszewski, *Mathematical Modeling of Tracer Experiments in Fissured Aquifers*, (Freiburger Schriften zur Hydrologie, Vol. 2, published by Universität Freiburg, Freiburg, Germany, 1994).
20. G.W. Walkup and R.N. Horne, *Characterization of tracer retention processes and their effect on tracer transport in fractured geothermal reservoirs*. SPE 1985 California Regional Meeting, Bakersfield, CA, 27-29 March, Society of Petroleum Engineers library record #13610, <http://www.spe.org>
21. J. Ramírez-Sabag, *A model to predict the tracer flow in naturally fractured geo-thermal reservoirs*, M. Eng. Thesis (in Spanish), School of Engineering, National University of Mexico, Mexico, 1998.
22. E.A. Sudicky and E.O. Frind, *Water Resour. Res.* **18** (1982) 1634.
23. P. Maloszewski and A. Zuber, *Interpretation of artificial and environmental tracers in fissured rocks with a porous matrix*. Proc. Isotope Hydrology 1983, Int. Atomic Energy Agency (IAEA), Vienna, Austria, 12-16 September, p. 635.
24. P. Maloszewski and A. Zuber, *Water Resour. Res.* **29** (1993) 2723.
25. F.R. de Hoog, J.H. Knight, and A.N. Stokes, *SIAM J. Sci. Stat. Comput.* **3**(1982) 357.
26. J. Ramírez-Sabag, O. Valdiviezo-Mijangos, and M. Coronado, *Geofísica Inter-nacional* **44** (2005) 113.
27. Z. Dai and J. Samper, *Water Resour. Res.* **40** (2004) W0747-1; doi:10.1029/2004 WR003248.
28. P.A. Lapcevic, K.S. Novakowski, and E.A. Sudicky, *Water Resour. Res.* **35** (1999) 2301.
29. C.L. Jensen, *Matrix diffusion and its effect on the modeling of tracer returns from the fractured geothermal reservoir at Wairakei, New Zealand*. SGP-TR-71, Report of the Stanford Geothermal Program, Stanford University, Stanford CA, 1983.
30. M. Mercado, C.E. Perez, M. Asadi, and D.R. Casas, *Gas-flow pattern evaluation: a successful inter-well field study*. SPE proceedings of the Latin American and Caribbean Petroleum Engineering Conference, Port of Spain, Trinidad, West Indies, 27-30 April 2003. Society of Petroleum Engineers library record # 81005, <http://www.spe.org>